Design and modeling of a piezoelectric micromachined ultrasound transducer

Colin McDonnell, Sarah Gontarek, Jakob Dahl

1 Introduction

Ultrasonic Imaging has been a standard and effective tool in medicine. Most commonly used to image during pregnancy, ultrasonic imaging can and has been used in an endless variety of settings[1]. In the MEMS community, there has been an intensive push towards creating micromachined ultrasonic transducers. This has two reasons: 1) Micromachined ultrasonic transducers (MUT) have much higher resonance frequencies than macroscale machines, making them applicable for imaging vascular and other small-scale structures and 2) micromachining has the potential to create much cheaper and more varied apparatus, even for intravenous catheter applications due to the small size of the transducer.

Various different designs have been put forward, though the two most distinct categories are distinguished by their method of actuation: capacitive or piezoelectric. We will not elaborate on the difference here - an excellent review of the methods and their relative utility is given by Neumann et al.[2] For our device, we decided to use a PMUT incorporating a piezoelectric polymer due to the ease in processing and use of low-temperature fabrication. The polymer, PVDF-TrFe has received much attention in recent years and there is a strong drive towards creating micromachined PVDF-TrFe ultrasonic transducer, even if it has been met with somewhat limited success[3]. However, the high sensitivity of PVDF allows the possibility of low-power transduction and sensing, which is desirable for efficiency and safety. In this paper, we attempt to design an ultrasonic transducer based on PVDF-TrFe and simulate the utility of this design for medical imaging.

---

[1] Tole, Nimrod M, and Harald Ostensen. "Basic physics of ultrasonic imaging." (2005): 39-47.

[2] Neumann, John J, David W Greve, and Irving J Oppenheim. "Comparison of piezoresistive and capacitive ultrasonic transducers." *Smart Structures and Materials* 29 Jul. 2004: 230-238.

[3] Chandrana, Chaitanya et al. "Design and analysis of MEMS based PVDF ultrasonic transducers for vascular imaging." *Sensors* 10.9 (2010): 8740-8750.

2 Mechanical properties of membrane

The mechanical model of our membrane was derived after the model in S. Shelton et al.[4] describing an AlN PMUT device. They developed a calculation based on energy methods to map the deflection of the membrane under the piezoelectric effect onto an arbitrary known membrane deflection function $w(r)$. Functions for the deflection profile were used from Wygant et. al.[5] describing the deflection profile of circular CMUT designs. While we are not operating under uniform loading, the deflection profile is likely to be quite similar. We used the equation: $w(r) = w(r)|_{peak} * (1 - r^2/a^2)^2$ to describe the profile of deflection (see Figure 1).

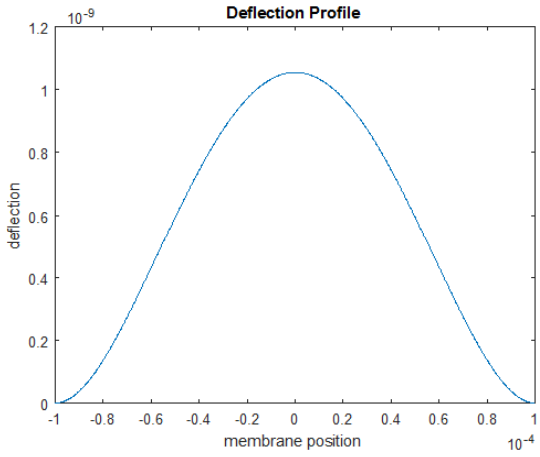

Finding the energetic minimum is accomplished by taking the derivative of an energy functional with respect to the deflection and finding the minimum, which yields:

$$w(r)|_{peak} = -(a^2/D * I_m/I_e)\, M = -(a^2/D * I_m/I_e)\, V_{in} * e_{31} * z_p$$

where a is the radius of the membrane, D is the flexural rigidity, I_m and I_e are energy functionals depending on the deflection profile, M is the piezoelectric bending moment, V_in is the input voltage, e_31 is the transverse piezoelectric strain coefficient and z_p is the distance from the midplane of the piezoelectric material to the neutral axis. The neutral axis was calculated according to a modified formula from the lecture notes:

Parameter	Value	Units
Radius	125	um
Total thickness	13.1	um
Neutral axis	5.55	um
Flexural rigidity	11.74	uN*m^2
Max deflection	0.14	nm
Resonance	0.33	MHz

$$z_{na} = z \text{ for which } \sum_{i}^{n} \int_{-zna}^{h-zna} E_p(i,z) * z\, dz = 0$$

where n is the number of layers, h is the height of the layer, E_p is the plate modulus of the layer, and z is the cumulative height from the bottom layer. The

[4] Shelton, Stefon et al. "CMOS-compatible AlN piezoelectric micromachined ultrasonic transducers." *Ultrasonics Symposium (IUS), 2009 IEEE International* 20 Sep. 2009: 402-405.

[5] Wygant, Ira O, Mario Kupnik, and Butrus T Khuri-Yakub. "Analytically calculating membrane displacement and the equivalent circuit model of a circular CMUT cell." *Ultrasonics Symposium, 2008. IUS 2008. IEEE* 2 Nov. 2008: 2111-2114.

flexural rigidity was calculated according to a formula from Nguyen-Dinh et al.:[6]

$$D = \sum_{i}^{n} \int_{h_{i-1}}^{h_i} E_p(i)\,(z - z_{na})^2 dz$$

To evaluate the energy model, we compared this to a bending moment-derived model , also from Nguyen-Dinh et al. In this case, the peak deflection was given by the following equation:

$$w(r) = \frac{M_p * R_{in}{}^2 * ln(R_m/R_{in})}{2\,D} = \frac{V_{in} * e_{31} * \int_{hpiezo}^{hpiezo+tpiezo} (z - z_{na})dz * R_{in}{}^2 * ln(R_m/R_{in})}{2\,D * t_{piezo}}$$

where M_p is the piezoelectric moment, R_in is the radius of the electrode, R_m is the radius of the membrane, D is the flexural rigidity, $tpiezo$ is the thickness of the piezoelectric layer and $hpiezo$ is the position of the piezoelectric layer from the bottom of the membrane. Effective spring constant and mass are

$$k_{eff} = \frac{192\pi}{R_m{}^2} D \quad , \quad m_{eff} = \frac{9\pi}{5} \sum_{i}^{n} \rho_i t_i * R_m{}^2$$

which gives rise to a natural resonance frequency given by

$$f_0 = \frac{1}{2\pi} \sqrt{\frac{k_{eff}}{m_{eff}}}$$

While the methods of calculation are very different in terms of theoretical foundation, the two methods give almost identical results for our system. As an example, the change in frequency and maximum displacement for the two different methods are given here. This gives us an important verification for our analytical calculations.

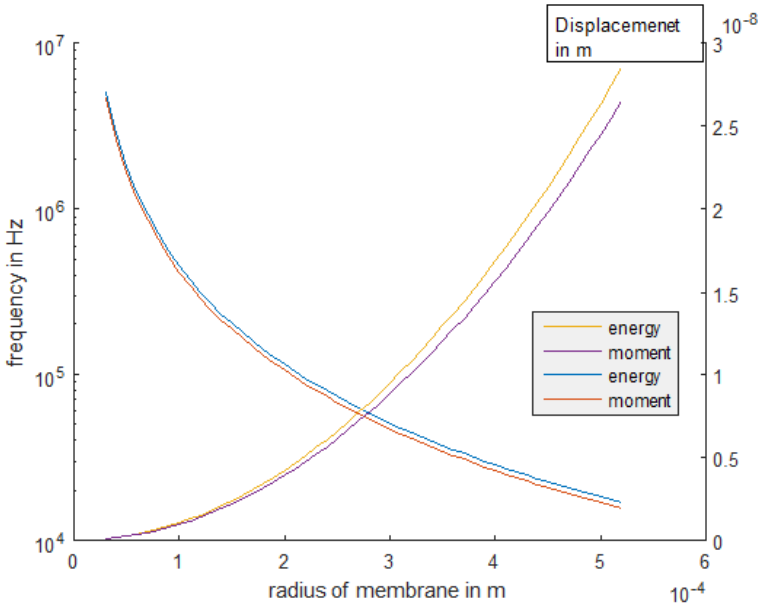

A straightforward polar integral over the radial displacement function gives us the total volumetric displacement for a given cycle of the membrane. By taking this V_v and treating the entire transducer as a cylindrical piston that oscillates with an amplitude of w_{peak} , we can calculate an effective area A_m which will be useful for acoustic calculations in the dynamic model.

[6] Nguyen-Dinh, An et al. "pMUT for high intensity focused ultrasound." *Ultrasonics Symposium (IUS), 2012 IEEE International* 7 Oct. 2012: 1-5.

3 Equivalent Circuit Model

We used an equivalent circuit model described by Przybyla et al., shown below.

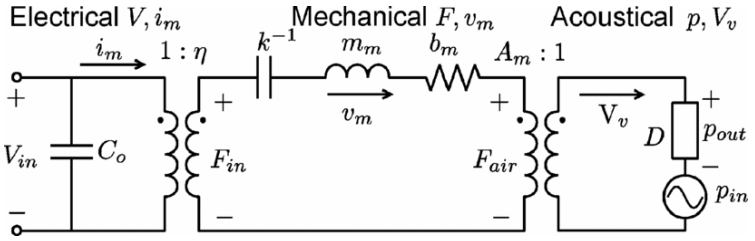

This circuit models the electromechanical interface and acousto-mechanical interface using lossless transformers to convert between effort sources (voltage, force, pressure) and flow sources (current, velocity, volumetric flow). The left domain of the circuit represents a true electrical voltage applied across a layer of piezoelectric with capacitance C_0. The middle section represents the mechanical domain, which includes a mechanical spring representing the transducer membrane, an inductor representing the inertia of the membrane mass, and a resistor modeling mechanical losses. For simplicity, we ignore this term in the analysis. Lastly, the rightmost domain represents the acoustic power being both radiated away by the impedance D and sensed by the voltage source p_{in}.

3.1 Electrical parameters

The only electrical parameter is C_0, which is the actual capacitance of the piezoelectric disk, given by $C_0 = e_r e_0 A/d$ where e_r is the relative permittivity of the piezoelectric material, e_0 is the permittivity of free space, A is the area, and d is the thickness of the layer.

3.2 Mechanical parameters

Using the energy methods described by Shelton, we derived the deflection

$$w(r)|_{peak} = -(a^2/D * I_m/I_e) V_{in} * e_{31} * z_p$$

This can be broken down into constituent elements that give us information regarding quantities in our circuit model. We see that $w_0 = \varphi C_m V$, where C_m is the mechanical capacitance in our model. This can be inverted to give us an effective spring constant k_{eff}. The constant φ represents a conversion factor from the electrical to mechanical domain, given by $\varphi = \pi I_M e_{31,f} z_p$. Finally, V is simply the maximum applied voltage.

We can calculate the natural unbiased resonant frequency $\omega_s{}^2 = \frac{\lambda_{01}}{a^4}\left(\frac{D}{\mu}\right)$, from which we can derive an effective mass according to $\omega_n^2 = \frac{k}{m}$. This defines the inductance of our mechanical inductor.

To calculate the damping in our mechanism and characterize an impulse response, derive the quality factor and bandwidth, we estimated the mechanical impedance of our device using the model described in Smyth [1]:

$$p_f = \frac{1}{2}\left(\frac{\omega}{\omega_{01}} - \frac{\omega_{01}}{\omega}\right)$$

$$k_1 = \sqrt{\frac{\sqrt{d^2 + 4c\omega} - d}{2c}}$$

$$k_2 = \sqrt{\frac{\sqrt{d^2 + 4c\omega} + d}{2c}}$$

$$Z_m = \frac{F}{u_\omega} = j\omega I_0' \frac{ak_1k_2\left[k_2J_0(k_1a)I_1(k_2a) + k_1J_1(k_1a)I_0(k_2a)\right]}{ak_1k_2\left[k_2J_0(k_1a)I_1(k_2a) + k_1J_1(k_1a)I_0(k_2a)\right] - 2\left(k_1^2 + k_2^2\right)J_1(k_1a)I_1(k_2a)}$$

We approximated many of the values in the above equation assuming that our operational frequency would be slightly under the estimated resonance frequency of our device, and assuming that our device would have a resonance frequency high enough to meet the problem specifications.

3.3 Acoustic parameters

The acoustic impedance is given by

$$D = \frac{\rho c}{A_m}\left(1 - \frac{2J_1(2wa)}{2wa} + j\frac{2K_1(2wa)}{2wa}\right), w = \frac{2\pi}{\lambda}.$$

where $J_1(*)$ is a first-order Bessel function, $K_1(*)$ is a first order Struve function, rho and c are the density of and speed of sound in the material surrounding the transducer, respectively. To convert D into the circuit domain, we multiply it by A^2/phi^2.

3.4 System dynamics

Using the calculated circuit parameters, we constructed transfer functions that modelled the system both in sensing mode and actuating mode. The system is represented as a simple two-terminal circuit, and the complex impedance of each component is known. The transfer function relating input current to input voltage we found to be

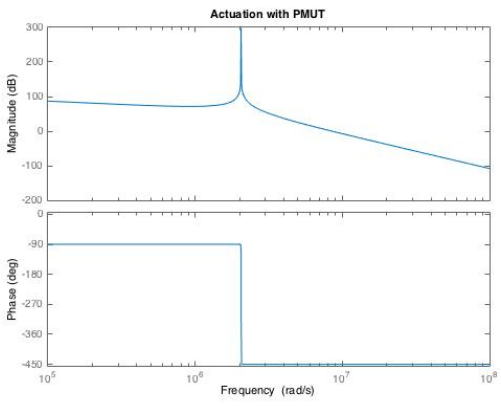

$$\frac{I_{in}}{V_{in}} = \frac{\varphi^2 C_0 s^2 + [DA^2{}_m + m_{eff}]s + k}{C_0 m_{eff} s^3 + C_0 DA^2{}_m s^2 + C_0}$$

Similar transfer functions were found for $\frac{p_{out}}{I_{in}}$, $\frac{V_{in}}{I_{in}}$, $\frac{I_{in}}{p_{out}}$. As these are all transfer functions of LTI systems, they can be multiplied together and remain valid. Thus, to calculate the overall transfer function $\frac{p_{out}}{V_{in}}$, it is possible to multiply $\frac{I_{in}}{V_{in}} * \frac{p_{out}}{I_{in}}$ and the I_{in} terms cancel, leaving the desired transfer function.

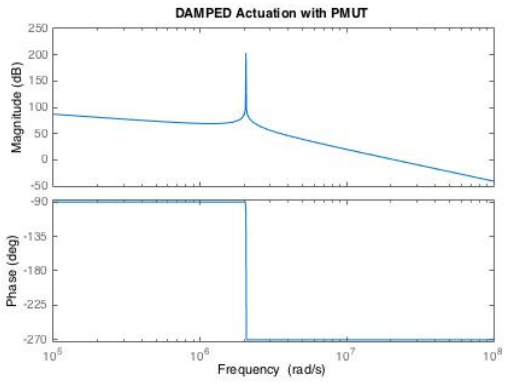

Parameter	Value	Units
C_0	2.09	nF
C_m	19	uF
m_eff	1.19E+01	nH
Z_acoust	1.8	Mohms
phi	1.38E-06	V/N
A_m	1.64E-08	N/Pa

We see a distinct spike in the transfer function at the resonance frequency of about 2MHz. The steepness of the spike occurs because there are no loss mechanisms in the model to damp out large oscillations. We added a mechanical impedance that introduced losses whenever the transducer membrane moved. Our model for the mechanical impedance is shown in the previous section.

Note that the transfer function with damping exhibits far smaller frequency response across the entire frequency spectrum. The effect is most pronounced at the resonant frequency, where there is a difference of over 100dB between the damped and undamped case.

4 Production

4.1 Fabrication process

In the fabrication process, we take advantage of the precision of soft lithography molding techniques as well as shadow masks for evaporation of gold and chromium layers. Fabrication processes for stamps and shadow masks are described shortly at the end of this section.

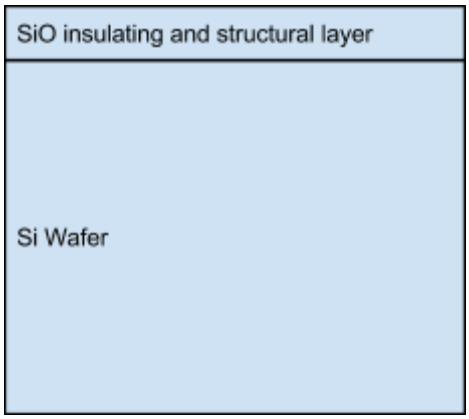

1. A 1 um thermal oxide layer is grown in a 800C oven for n minutes.

2. A shadow mask is placed on top of the wafer and a 500 Angstrom layer of titanium and a 2500 Angstrom gold layer is sputtered on. The radius of the electrode is 100 μm.

3. PVDF-TrFE is spun coated on to the wafer and a prefabricated stamp is used to mold and form the polymer. The polymer is cured in the mold at 130 C.

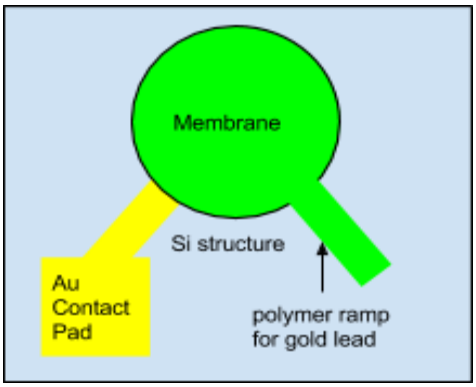

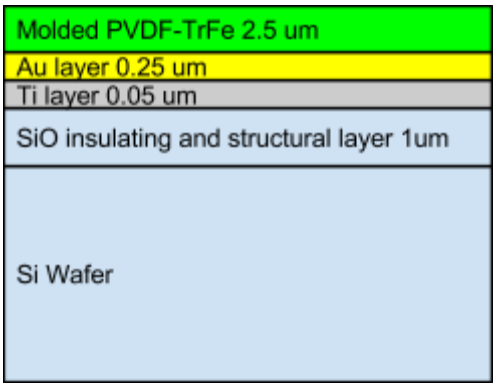

4. A shadow mask is placed on top of the wafer and a 500 Angstrom layer of titanium and a 2500 Angstrom gold layer is sputtered on.

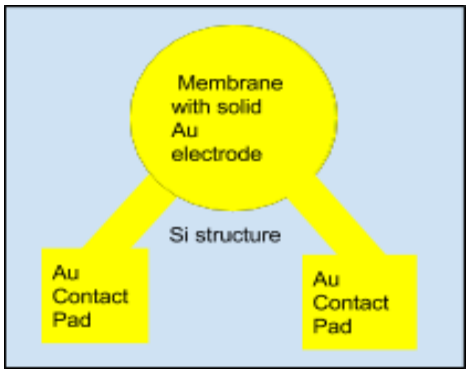

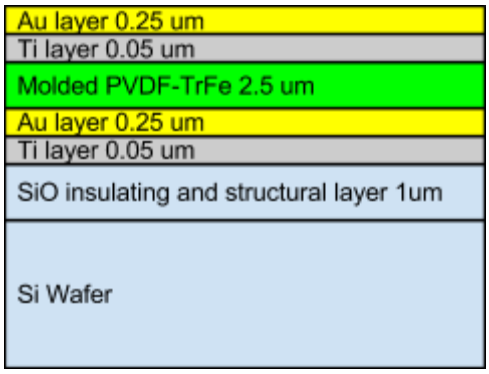

5. Reverse Side DRIE etching of the wafer until the SiO etch stop is reached. The fluoropolymer etch stop is not removed at the end of the DRIE process, as this would also remove the polymer membrane.

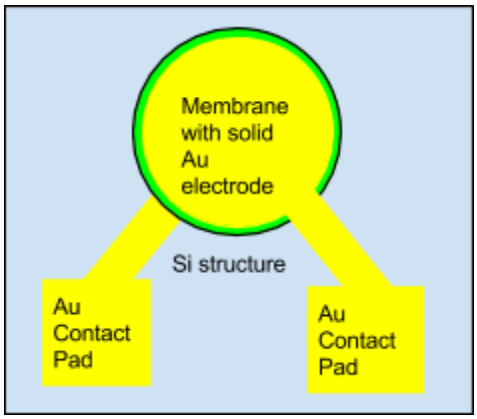

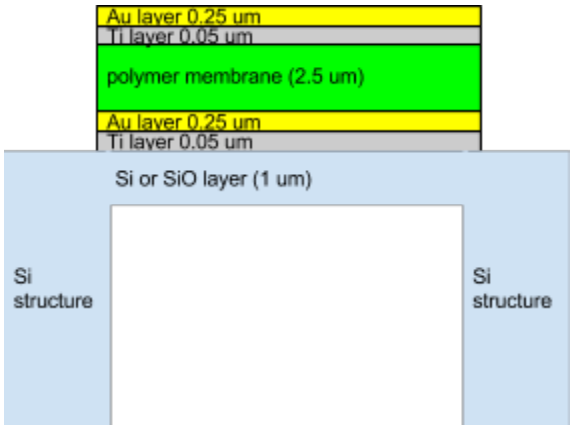

The 25 um radius membranes will be spaced 50 um apart, so that one pixel takes up 100 um side length. To create maximum viewing space and resolution, there will be 18 ultrasonic pixels on one device with side lengths of 1.9 mm * 0.5 mm. Since the structure is relatively resilient, a die saw process is used to release the devices.

4.2 Fabrication of the stamp

Deposit SiN (0.5 um) on a SOI wafer (top layer: 2.5 microns silicon). Spin on photoresist, and use lithography to define a square of 12 um side length aligned in the [110] direction. Etch with hot phosphoric acid, then etch the square with KOH. This produces a square hole with ramped edges. Spin casting a thick layer of polymer resist of around 5 um. Use lithography to define a circle of n um radius, then DRIE etch until the insulator layer has been reached. Ash all resist, then etch all the SiN layer with hot phosphoric acid.

4.3 Fabrication of the shadow mask

The form can be etched through on a thin (10 - 30 um) silicon wafer using DRIE after patterning with photoresist. Since the etch is going through the wafer, the different etching rates for the different sized parts don't truly matter - the etch is simply continued to completion.The size of the shadow mask holes defines the area of the electrodes.

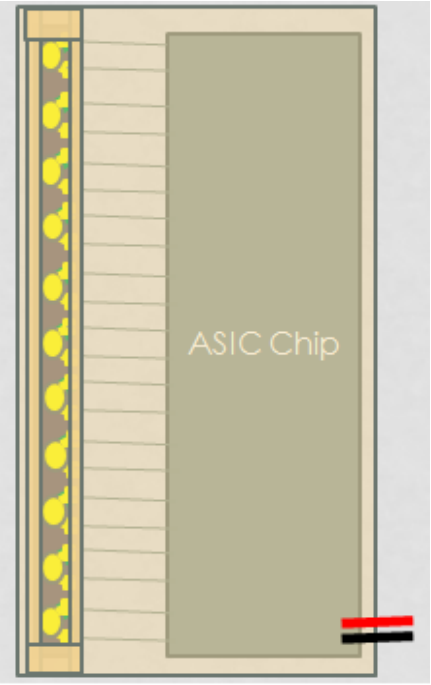

4.4 Device integration

We are using a two-chip implementation: one MEMS chip with 8 transducers created through the fabrication process we have just defined and one ASIC chip. The ASIC unit will have the signal processing and generating hardware defined previously. Wire bonding will be used to connect the MEMS and the ASIC chip electronically and to the outside framework.

5 Packaging

5.1 Coating

In order to protect patients from the voltage and the device from bodily fluids, the wafer can be cast directly into a polyethylene die. Polyethylene has been widely used in clinical applications such as hip prostheses and has a recorded history of very slow erosion even when mechanically strained in the body over a period of years. Maintaining the correct orientation is key to this process, so that air pockets remain on the backside of the MEMS chip - chip must be placed with the backside facing down, so that the air is trapped and sealed inside.

5.2 Toxicity

In the device, no metals are used that can produce toxic oxides. For the process, this means substituting Chromium adhesion layers with Titanium, since this will ensure that even if bioleaching occurs, no toxic Chromium salts are released. This also favours our choice of an insoluble poly (vinylidine difluoride/trifluoride) polymer versus the standard lead zirconium titanate, which could release toxic lead salts. While this would not be much of an issue during standard operation, in a worst case scenario of the device falling off of the instrument and becoming enclosed in human tissue, ensuring that all the parts are non-toxic definitely improves the outcome.

5.3 Voltage shock safety

To protect patients from device shock, the packaging is made from a non-conductive material. Any plastic will provide the necessary resistance to shock, and the use of glycerol matching fluid ensures that there is no large fluidic electrical conductivity.

5.4 Biocompatibility

Patients will mainly be exposed to polyethylene surface of the device. Polyethylene is ubiquitous in our daily lives and has also been used widely in clinical applications. While PE is not biodegradable, it is definitely biocompatible and will not harm patients even if used for intravenous applications.

6 Anticipated Performance

How our device fares on specification criteria.

A. Chip Size
B. Axial Resolution
    a. We estimated our axial resolution in the best case to be $\lambda = \frac{c_{tissue}}{\omega_0}$, $SPL = \lambda * \#\, cycles\ per\ pulse$ because our damping and Q are very good, we do not expect to have much ringing artifacts, allowing us to have only one pulse per cycle. Therefore $SPL = \lambda * 1 = 0.0007 = 2 * AxialResolution$ This puts our axial resolution at 350 microns, which admittedly is 5 times larger than the fidelity called for in the specification. However, by continuing to adjust parameters to raise the resonant frequency, we believe that a 5-fold increase in resolution may be possible.

C. Imaging Depth
    To calculate our imaging depth, we found the acoustic reflection rate at the interface between brain tissue and air, by taking the acoustic impedances of both materials from

a medical text [4], and using the following formula (other tissues and blood were also similar): $reflect\,\% = \frac{(Z_{t1} - Z_{air})}{Z_{t1} + Z_{air}}$ = 99.98% for a brain tissue-air interface.

We then found the appropriate sound power attenuation factors to account for the 2mm distance travelled in both directions by a received ping.

$P(x + \Delta x) = P(x)e^{-\alpha(\omega)\Delta x}, \alpha(\omega) = \alpha_0\omega^{\eta}$, where a(w) is unique to the material and frequency.

We found literature that had prepared tables of a(w) values, and used a value of α_0 at 2MHz for fatty neurological tissue: 0.35 [5]

Using this, our propagation loss of power over four millimeters (the specified image depth constraint) is (1 - 0.998) times the original signal power.

Our cumulative loss of signal in this use case should be no more than a few percent, less than one tenth of our original power. This is easily within the transducer's sensing capacity.

D. Bandwidth

The bandwidth of our device is definitionally inversely proportional to the quality factor. We compared two methods for calculating the quality factor based on

Smyth [1]: $Q = \frac{1}{2p_f}\frac{X_m + X_a}{R_m + R_a}$

and Pryzbyla [2]: $Q = \frac{(k_{eff} * \omega_0)}{(\varphi * V)}$, $where\ V = 5V\ bias\ voltage$

We found that Q was roughly 1, making our fractional bandwidth Q^{-1} = 100%

E. Impedance Ratio with Tissue

F. Voltage Supply

We calculated all parameters and modelling with the assumption that there would be a 5V source available to bias our device.

G. Beam Forming/Steering

We plan to have our transducer array be controlled by connected custom ASICs, which will be designed to be able to emit synchronized variable-phase pulses to perform beam steering. Our relatively large mechanical damping allows for short pulse lengths which creates a lot of flexibility for varying levels of phase delay during the small up time of the duty cycle.

H. Microfab (see next section)
I. Biocompatibility

   For packaging, we have decided to completely encase our device in PDMS (otherwise known as medical-grade silicone). This material has excellent impedance matching with tissue and provides a protective hydrophobic and shock-resistant coating for the sensitive electronics within.

J. Noise analysis:

Thermal noise from circuits: Thermal noise from IC and other circuitry is generally estimated to be around 20 μV. Assuming we have a 100 kΩ resistance in the circuit and a bandwidth of 100 kHz, the noise is given by $V_n = \sqrt{4k_bTRB}$, which comes out to around $10\mu V$.

Thermal-mechanical noise. The thermo-mechanical noise force is given by $F_n = \sqrt{4k_bT\omega_0 M/Q}$ which gives us a theoretical accuracy of $2 * 10^{-14}\, m$ or around $100\mu V$ While it is clearly impossible to measure those lengths precisely, it is also clear that the mass we are using is too large to be disturbed too much by thermal noise. Even with an overly cautious resolution limitation of 1 mV, we can safely measure signals that are 5000x smaller than our output signal.

Conclusion: While it is definitely possible to create a PVDF-TrFe polymer based ultrasonic transducer, as referenced previously, the design constraints for vascular imaging make this a very difficult problem. More work on device architecture and a strong optimization procedure is needed before MHz frequency operation of a micromachined polymer transducer becomes truly feasible.